Multi-Objective Optimization of High Power Diode Laser Surface Hardening Process of AISI 410 by means of RSM and Desirability Approach

Mahmoud Moradi[1, 2 *], Hossein Arabi[1, 2]

1-Department of Mechanical Engineering, Faculty of Engineering, Malayer University, Malayer, Iran

2-Laser Materials Processing Research Center, Malayer University, Malayer, Iran

Abstract:

In this research, laser surface hardening of AISI 410 was carried out by a high power diode laser based on Response Surface Method (RSM). Laser power, scanning speed, and focal plane position were evaluated as input process changeable while geometry dimensions of hardened zone (i.e., Depth and Width of hardness), maximum hardness, Microhardness deviation (MHD) from base material in depth and width, and ferrite phase percentage in the microstructure were evaluated as process output Results. The effect of input parameters on the response variations were studied by statistical investigation. Microstructure evaluation of the laser hardened zone was carried out through optical microscopy. Results indicated that by increasing the laser power and decreasing other parameters, higher surface hardness with significant penetration, and least ferrite percentage would be reached by means of the desirability function approach. By using experimental tests, validation of optimized results was performed.

Keywords: Laser Materials Processing; Laser Surface Hardening; High Power Diode Laser; Design of Experiments; Optimization.

1. Introduction

Commented [M1]: Az in ghesmat kheili kam konid
Na inke paper ha ro hazf konid...

FAGHAT tozihat e ezafi ro hazf konid ke nesf she
Vali ensejam e koli bemoone hatman...

The conventional surface treatment processes possess several limitations, i.e., high time and energy consumption, intricate heat treatment schedule, larger heat affected zone, lack of solid solubility limit and slower kinetics. Furthermore, few of the above-mentioned techniques are not environment friendly [1]. Laser processing is used for various applications such as laser welding and brazing [2-6], laser drilling [7, 8], laser cutting [9] and laser surface hardening [10-13]. A diode laser is one of the public laser types in industry. This type of laser with high accuracy heat treats the surface of the matter. Experiments based on trial and error takes a lot of time and Design of Experiments (DOE) not take into account the interactions of the parameters and cause a lot of mistakes. Recently, DOE has been developed in various experimental works [14-15]. Reducing the number of experiments, taking into account the interactions effects and developing mathematical functions to achieve the logical relationship between input and output parameters are the advantages of the RSM methods [16 -17].

Lo et al. (2003) [18] conducted a study on the surface hardening of AISI 440C martensitic stainless steel with Nd:YAG high power laser. A hardened layer of several hundred microns thick, consisting of martensitic phases, residual austenite, and carbides was created. Microstructure and the hardened layer due to optimal laser parameters reached to 600-800 Vickers hardness. Bressan et al. (2008) [19] investigate the influence of hardness on the abrasion resistance of 17-4 ph martensitic stainless steel. They used the pin and the plate to measure the wear resistance of the material obtained by conventional melting. Results showed that 17-4 ph martensitic stainless steel after the laser hardening was demonstrated a very nice wear resistance compared to the base material. Mahmudi et al. (2008) [20] conducted a study on martensite steel AISI 420 by laser Nd:YAG. In optimal conditions, by changing the effective parameters, they could increase the surface hardness up to 2.5 times the annealed steel state and increase with a hardness of 90% the maximum hardness of furnace hardening heat treatment. Mahmudi et al. (2010) [21] performed hardening of the AISI 420 martensitic stainless steel by Nd:YAG solid-state lasers. They investigated the effects of process parameters (beam energy, pulse duration, and scanning speed) on hardness, geometrical dimension, and the microstructure of hardened zone. Overlapping tests were conducted, and the corrosion resistance on hardened laser samples was evaluated. The highest hardness was reported about 500 Vickers at a depth of 200 microns. Badkar et al. (2010) [22] studied the surface hardening of pure titanium metal by 2 kW Nd:YAG laser. Influences of the laser power, the scanning speed, and the focal point position were studied. The geometric dimensions (depth and width of the hardened area) as well as the curvature angle of hardened area were surveyed using the RSM method. Li et al. (2014) [23] were performed a study on the surface hardening of AISI 1045 using two different types of lasers: a high power diode laser with the power of 3.5 kw, and a CO_2 laser with the power of 15 kw. The results of this study showed that the geometry of the hardened area by using a high power diode laser is higher than the CO_2 laser. Also the angles caused by the curvature of the hardened area using the response surface method were surveyed. Cordovilla et al. (2016) [24] by simulating the laser hardening process and comparison the results obtained from the laser hardening simulation process with the experimental data of the laser hardening of AISI 4140 low alloy steel. They have investigated the effect of overlapping of hardened layers.

Commented [M2]: Bayad in ghesmat ro ta jayee ke mishe becheloonid....

Har paper ro alan 3-4 khat tozih dadid... 1-2 khat she
Va inke momkene 2-3 ta paper ro betoonid dar yek jomle sharh bedid...
Ke dige tartib refrence ha ham beham nakhore dige....

Martensitic stainless steels are used in several industries includeing petroleum, gas and petrochemical, food and pharmaceutical. These alloys are used in manufacturing corrosion resistance pipes and plates and applied in an acidic environment which are more economical than similar grades [25]. The applications of AISI 410 martensitic stainless steel are used in low-pressure steam turbine blades in power plants. Other common uses in the production of petrochemical gates, jet engine parts, compressor components, valves and a variety of pumps [26]. Because of these wide ranges of industrial application AISI 410 martensitic stainless steel is selected as the material workpiece in this study.

Notwithstanding the great efforts by various researchers, many aspects related to laser hardening of steel alloys are still unsolved and much more research should be carried out with the aim of increasing the depth and hardness values. According to the literature, diode laser is a good candidate for this goal. In this paper, RSM method is used to study the effects of the diode laser surface hardening process variables, i.e. the laser focal plane position (FPP), the scanning speed (S), and the laser power (P), on the geometry of hardened layer and surface hardness distribution in the samples of AISI 410 stainless steel by Design Expert software. Optimizing the laser hardening parameters was done to obtain desired results. To validate the optimization results, three lasers hardening experiments were conducted at optimum settings.

2. Experimental work and methodology

DOE is a method of examining the effects of multiple variables on output variables (responses). DOE involves an experiment or a series of experiments that purposely improve the input parameters in the process to be observed and detected by the amount of variation in the output response of the process [27-28].

Commented [M3]: Niaz nist
Yek khat faghat dar paragraphe badi be noyee begid ke eshare shode bashe
Pas in ro hazf konid.

In the present work, laser focal plane position (FPP), the scanning speed (S), and the laser power (P) were considered as independent input variables. Table 1 shows three input parameters of the experiment, coded and actual values of their levels.

Table. 1 Independent process parameters with design levels

Variable	Notation	Unit	-2	-1	0	1	2
scanning speed	S	[mm/s]	4	5	6	7	8
Laser power	P	[w]	800	1000	1200	1400	1600
Focal plane position	FPP	[mm]	60	65	70	75	80

In this study, to carry out the tests, central composite design (CCD) five-level RSM design with three parameters, presented in Table 2, were done.The experimental design contains 17 experiments which contain eight experiments as factorial points in the cubic vertex, six experiments as axial points and three experiments in the cubic center as center point experiments. [29-30]. AISI 410 martensitic stainless steel was considered as a material work piece in this study, with the chemical composition presented in Table 3, which is the average of three X-ray fluorescence (XRF) measurements. Specimens with a thickness of 10 mm from a rod of 65 mm in diameter were prepared by machining, and the surfaces of the specimens were ground.

Commented [M4]: Inam kholase mishe kard

Semiconductor continuous wave diode laser with a maximum power of 1600 W was used as a laser source in the laser surface hardening experiments. The wavelength of the used diode laser is 808 nm. Trial specimens of laser hardening were performed by changing one of the process variables to determine the working range of each parameter. Laser hardening experiments were carried out according to the matrix design presented in Table 2. Figure 1 shows a schematic of the laser hardening mechanism. Figure 2 depicts the images of hardened laser samples. After laser hardening, samples were sectioned from the middle of the hardened line. To prepare the metallographic samples, cut specimens were mounted in a phenolic thermosetting resin, conventionally grounded, polished and etched in the villa's reagent (C6H3N3O7 2gr, Hcl 5cc, C2H5OH 100cc) [30]. The geometry features of the hardened layer (width and depth), as shown in Figure 3, were measured using BUEHLER MET B7 optical microscope at a magnification of 200X and the images were analyzed by the ImageJ software.

Commented [M5]: In paragraph ham mishe jomalati ro hazf kard
Va bazi hash ro kholase tar konid.

Table 2. Experimental layout and results

Test no	Input parameters			Output results					
	Scanning speed (mm/s)	Focal plane position (mm)	Laser power (W)	Maximum hardness (HV)	Depth of hardness (mm)	width of hardness (mm)	MHD in depth	MHD in width	Ferrite percent (%)
1	5	65	1400	600	2.2	8.1	18658.42	26621.6	0.5
2	8	70	1200	478	0.5	9.2	11421.1	9459.87	3.1
3	6	70	1200	488	1.3	8.5	12336.5	16404.63	0.8
4	6	70	1200	490	1.4	8.4	12399	16417.13	1.9
5	6	60	1200	520	2.2	8.1	15090.5	20074.5	1.5
6	6	80	1200	470	0.6	9.1	10532.44	7782.8	3.34
7	7	75	1000	500	0.8	8.9	12287.71	15853.7	2.2
8	7	65	1000	508	0.9	8.85	12407.13	16560.4	2.53
9	5	75	1000	510	1	8.75	12346.13	16027.6	1.65
10	5	65	1000	515	1.1	8.6	12711.89	16890.1	1.3
11	7	65	1400	540	2.2	8.1	16211.64	21364.2	0.5
12	6	70	1200	500	1.5	8.65	12492	17042.8	1.4
13	6	70	1600	620	1.8	8.3	18813.7	28651.6	0.62
14	7	75	1400	512	1.3	8.5	12816.89	17560.4	0.76
15	4	70	1200	530	2.3	8.01	16053	20813.7	1
16	6	70	800	478	0.7	9	10204	7493.2	2.8
17	5	75	1400	530	1.8	8.3	15311.9	18355.2	2

Table. 3 Chemical composition of AISI 410 stainless steel (Wt. %)

Element name	C	Mo	Cr	Cu	S	P	Mn	Ni	Si	Al	V	Fe
Weight percent	0.15	0.03	13.5	0.11	0.024	0.018	0.51	0.12	0.28	0.008	0.021	Balance

Figure 4 illustrates the influences of the input parameters variations on the hardened layer geometry of some selected experiments listed in Table 2. The microstructure was observed by optical microscopy (OM). Celemex software was used to measure the percentage of the ferrite phase in the structure of the hardened layer. Microhardness measurements were performed along a line 30 µm below the top surface on the transverse cross- section of the hardened zone using a micro-indentation tester (BUEHLER, USA). The measurements were taken by using a maximum load of 100 gr and a dwell time of 30 s. Microhardness tests were repeated at least three times for each sample. The hardness profiles along the line from the middle of the hardened zone to the base metal in depth and width directions of the hardened zone were plotted for each sample [31, 32].

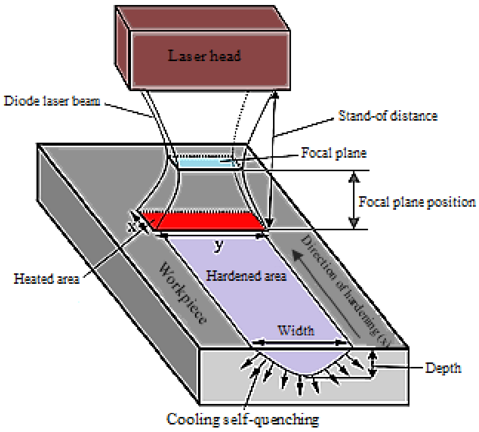

Fig.1. A schematically image of the laser hardening [32].

Table. 4 The Incident beam (length, width and area)

Focal plane position	Incident beam length (x)	Incident beam width (y)	Incident beam area (xy)
60 mm	1.50 mm	8.00 mm	12.00 mm^2
65 mm	2.55 mm	9.94 mm	25.34 mm^2
70 mm	3.60 mm	11.88 mm	42.77 mm^2
75 mm	4.65 mm	13.82 mm	64.30 mm^2
80 mm	5.67 mm	15.76 mm	89.36 mm^2

By dividing the incident beam length (x) to the scanning speed (S) the interaction time is calculated, Equation 6 [32-33]. Figure 1 and Table 4 present the incident beam length (x). The beam density will be obtained by dividing the laser power to the incident beam area, presented in Table 4, Equation 7 [32-33].

$$\text{Interaction time} = \text{Incident beam length (x)} / \text{Scanning speed (S)} \quad (6)$$

$$\text{Beam density} = \text{Laser power} / \text{Incident beam area} \quad (7)$$

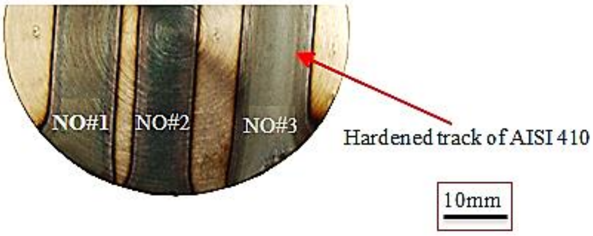

Fig. 2 An image of hardened laser tracks

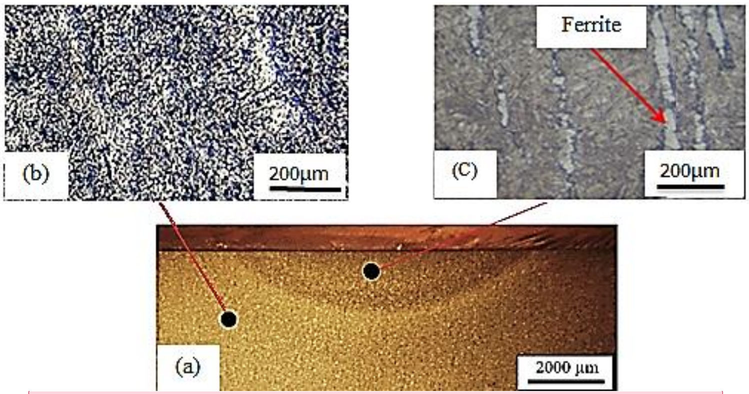

Fig. 3 Image of geometrical dimensions of the hardened zone (width and depth)

Commented [M6]: In ax va tozihatesh ro hazf konid kolan....

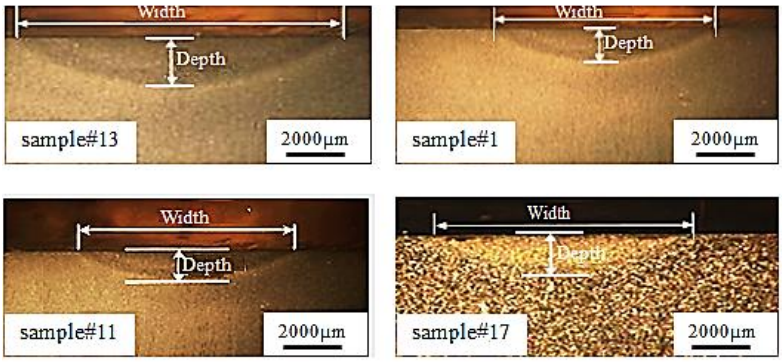

Fig. 4 Effect of the input parameters variations on the geometry of the hardened layer

Commented [M7]: In ax ham 2 tash bashe kafie ke hajm paper kam she

The microhardness deviation from base metal microhardness (MHD) is obtained from Equation 8 [34]:

$$\text{MHD}=\sum_{i=1}^{n}\frac{(x_i-x_{b.m})^2}{n} \tag{8}$$

Where, x_i is the microhardness of different points and $x_{b.m}$ is the microhardness of the base metal, and n is the number of points that their microhardness is measured**.** In this research n is 10 and $x_{b.m}$ is equal to 330 Vickers. According to Equation 8, the MHD parameter has a direct relationship with hardness. Therefore, with increasing the hardness, MHD parameter also increases. In the laser hardening process, having higher MHD values is more desirable. Higher MHD parameter in the hardened sample indicates the higher uniformity of the hardness profile in the hardened area.

Commented [M8]: In ezafast.
Barasish konid o hazfesh konid....

3. Results and discussion

The maximum hardness of the hardened zone, geometrical dimensions (depth, width) and microhardness deviation (MHD) from base material in depth and width and percentage of the ferrite phase in the microstructure were measured as the output responses of the experiment. Analysis of variance (ANOVA) was used to investigate significant effective parameters on laser hardening process and interpretation of the results in these analyses, full quadratic polynomial functions were employed using Design Expert software.

Commented [M9]: In ham kolan hazf she

3.1 Maximum hardness

As shown in Table 5, according to the Analysis of variance for the maximum hardness, all of the main parameters (laser power, focal plane position, and scanning speed) are effective. Among quadratic terms the quadratic term of laser power (P^2) is significant. The regression equation obtained is evaluated as significant, and Lack-of-fit as insignificant. According to the analysis performed on the modified model, in the best analysis, regression is to be significant and Lack-of-fit should be insignificant. Therefore according to the analysis in ANOVA Table 5, the final regression equation based on the coded and actual values, considering significant parameters is presented in Equations 9 and 10, respectively:

Commented [M10]: Az In 2 moadele faghat yeki ro bezarid
Coded valu ro
Ke hajme paper kamtar she
Baraye tamame khorooji ha moadele dovomi ro hazf konid pas....

$$(\text{Maximum hardness})^{-2.51}=+1.652E-007+1.811E-008\ S+1.964E-008\ FPP-3.470E-008P-3.035E-008\ P^2 \quad (9)$$

$$(\text{Maximum hardness})^{-2.51}=-1.95703E-007+9.05705E-009S+1.96399E-009FPP+3.68469E-010P -1.89672E-013P^2 \quad (10)$$

Table. 5 Revised analysis of variance of maximum hardness

Source	Sum of squares	Degree of freedom	Mean square	F-value	P-value
Model	9.107E-015	4	2.277E-015	12.42	0.0003
S	1.312E-015	1	1.312E-015	7.16	0.0202
P	4.816E-015	1	4.816E-015	26.27	0.0003
FPP	1.543E-015	1	1.543E-015	8.42	0.0133
P^2	1.436E-015	1	1.436E-015	7.83	0.0161
Residual	2.200E-015	12	1.833E-016		
Lack of fit	2.136E-015	10	2.136E-016	6.69	0.1369
Pure error	6.383E-017	2	3.192E-017		
Total	1.131E-014	16			
	R-Squared= %.80.54		Adj R-Squared= %74.06		

R-sq. is the amount of the experimental data coverage that is obtained by regression Equations 9 and 10. Figure 5 shows perturbation plot of maximum hardness. The perturbation plot is used to compare the effect of all the input factors in the central point in the design space. The maximum hardness perturbation is plotted by changing only one parameter over its range while the other parameters are kept fix. Each line in this plot displays the sensitivity of maximum hardness to the input variables. From the perturbation plot, it is obvious that the laser power (P) has a direct effect while the focal plane position (FPP) and the scanning speed (S) have an inverse effect on the maximum hardness. This relation could be easily understood from the physical occurrences of the laser hardening process.

Commented [M11]: Kholase tar bayan she
Va az gheire zaroori ha ejtenab she

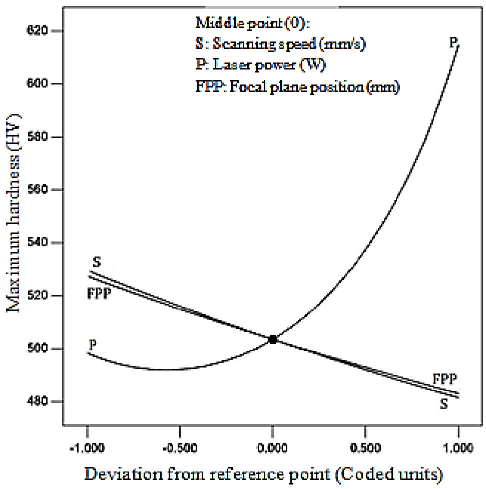

Fig.5 Perturbation plot of maximum hardness

Figure 6 illustrates the response surface plots of the maximum hardness. The concept of the beam density which is a function of the incident beam area presented in Table 4 and the red area in Figure 1 can be explained more understandable. When the beam is closer to the surface, focal plane position reduces, the incident beam area becomes smaller and the density of the beam will increases. As it is deduced from Figure 6-a by decreasing the focal plane position and scanning speed, the amount of input energy increases to the surface of the workpiece, so the maximum hardness increases. As shown in Figure 6-b the hardness increases with decreasing the scanning speed and increasing the laser power. The reason for this phenomenon is that laser energy increases with increasing laser power. Therefore the energy radiated to the hardened area increases and as a result, the maximum hardness increases. Decreasing the scanning speed increases the interaction time of the laser beam radiated to the workpiece surface, thus the maximum hardness increases. This phenomenon can be argued with the heat input, and Equation 11 describes the amount of heat input based on laser power and laser scanning speed [35].

Commented [M12]: Tozihat nesf she...
Gheire zaroori ha hazf shan

Heat input(J) = Laser power (W) / Scanning speed (mm/s) (11)

As can be seen, the heat input is directly related to increasing the laser power and reducing the scanning speed. With the same discussion mentioned for explaining Figure 6-a, b, and c, it could be used easily for better understanding.

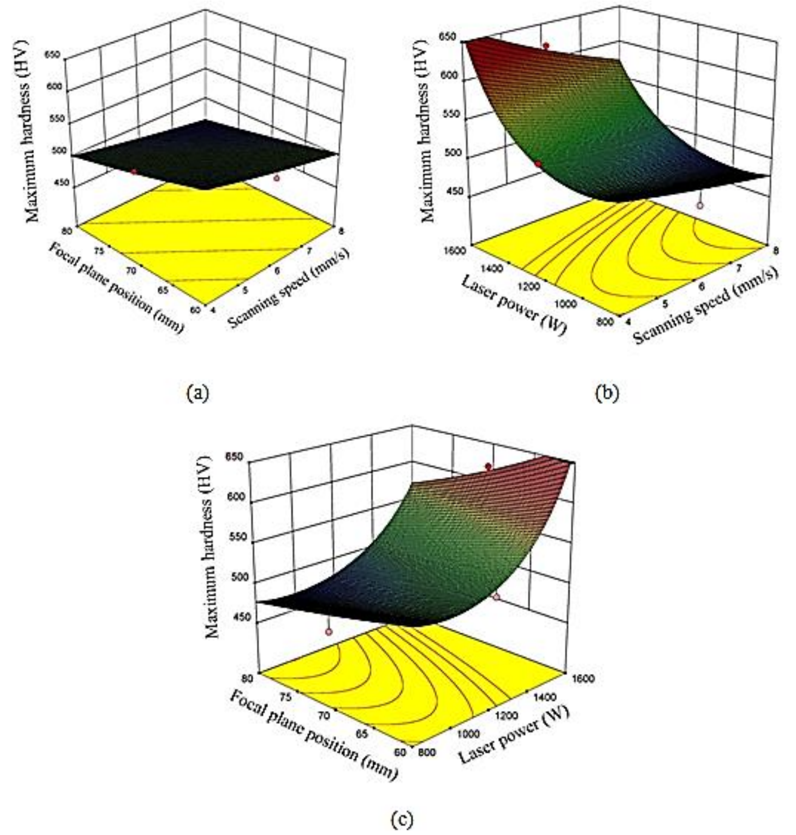

Fig. 6 Response surface plots of the maximum hardness

The normal plot of residuals for maximum hardness is displayed in Figure 7. As it is shown in the normal probability diagram, the response of maximum hardness, around the diagonal line, shows the normal distribution. So, the regression equation is a suitable model for predicting and investigating the effects of input parameters on the maximum hardness.

Commented [M13]: Kolan hazf she

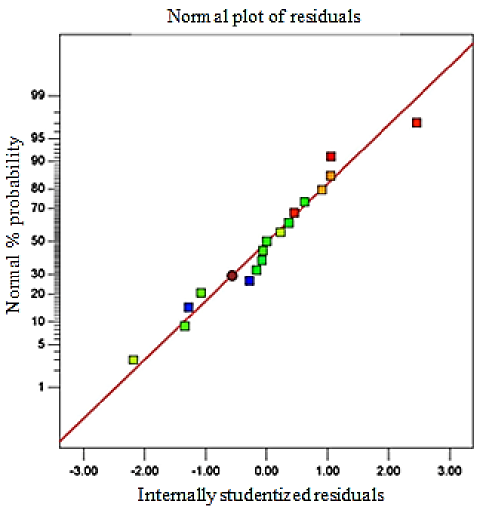

Fig.7 Normal plot of residuals for maximum hardness

Commented [M14]: In normal plot ha kolan hazf shan + tozihat dar matneshoon

According to the mentioned explanations, the reason for increasing the surface hardness of AISI 410 stainless steel can be expressed by physical phenomena, regarding the amount of heat energy transferred into the workpiece by laser radiation. In general, increases in surface hardness of the laser hardening process depends on the following factors [36]:

1. Amount of heat input to the workpiece surface.
2. The laser absorption coefficient which depends on the laser wavelength
3. The topology of the workpiece surface.
4. Grain size in the microstructure of samples.

Regarding the physical phenomena, by decreasing the wavelength of the laser, the amount of the laser beam absorption increases, and the reflection of the laser beam on the surface of the workpiece decreases. The diode laser beam with a wavelength of 0.808 nm, absorbs more thermal energy and gives more hardness to the surface of the workpiece. As shown in Table 6, the absorption coefficient of the diode laser is 45% without absorption coatings and 85% with absorption coatings [36]. So, by increasing in the absorption of the laser beam, the surface hardness and also the geometric dimensions of the hardened area increases.

Commented [M15]: In ro dar hade 2-3 khat kahesh bedid....
Kolesh ziad zaroori nist

Table. 6 Physical properties and absorptivity percent of AISI 410

Physical & termal properties	Density,lbs/ in^3(g/g/cm^3)	Thermal conductivity, BTU/hr/ft/(W/m/k)	Modulus of Elasticity, ksi. (Mpa)	Specific, Heat, BTU/lbs/ºF(kJ /kg/k)	Absorptivity,% [36] in diode laser	
					With absorption coatings	without absorption coatings
AISI410	7.74	24.9	200	0.46	85	45

3.2 The Depth of the hardened area

Table 7 shows a revised analysis of variance of the depth of hardened area. As can be seen, all of the main parameters are identified as a significant parameter, and other terms are insignificant. In ANOVA Table 6, Lack-of-fit is insignificant, so the overall model of the depth of the hardened area is effective, which indicates that proper analysis has been done. Regarding the performed statistical analysis, the modified regression equation in the form of coded values and actual values, are presented concerning the effective parameters in Equations 12 and 13 respectively.

Commented [M16]: Mesle tozihat ghabli yekish hazf she

Commented [M17]: In ham bebin mishe kholase tar she behtare

$$(\text{Depth of hardness})^{0.64} = +1.21-0.33\ S - 0.33FPP +0.43P \quad (12)$$

$$(\text{Depth of hardness})^{0.64} = +3.26564-0.16625\ S-0.033429FPP+1.06539E-003\ P \quad (13)$$

Table. 7 Revised analysis of variance of depth of hardened area

Source	Sum of squares	Degree of freedom	Mean square	F-value	P-value
Model	1.62	3	0.54	19.99	< 0.0001
S	0.44	1	0.44	16.42	0.0014
P	0.73	1	0.73	26.97	0.0002
FPP	0.45	1	0.45	16.59	0.0013
Residual	0.35	13	0.027		
Lack of fit	0.34	11	0.031	9.71	0.0970
Pure error	6.435E-003	2	3.218E-003		
Total	1.97	16			
R-Squared= %82.19			Adj R-Squared = %78.08		

Perturbation plot of the depth of hardness is shown in Figure 8. As shown in Figure 8 with decreasing scanning speed, the depth of hardness increases. The reason for this is that when the scanning speed reduced, the time of laser interaction on the surface of the workpiece is increased and surface is exposed to more heat, so the depth of hardness increases. Also, the depth of hardness increases by decreasing the focal plane position and increasing the laser power. It is obvious that with decreasing the focal plane position (see Figure 1) and increasing the laser power, the surface of the workpiece is exposed to more heat and more energy absorbs by workpiece surface, so the depth of hardness increases.

Commented [M18]: Bazi jomalatesh ro be tahlil haye ghabli dar tahlil khorooji ghabli eshare shode fek konam…
Pas inja 2 bare nagim
Va begim ke hamoontor ke dar bakhshe folan goftimeshooon….

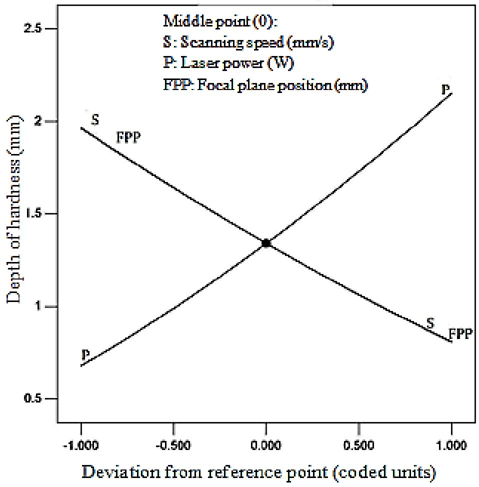

Fig.8 Perturbation plot of the depth of hardness

Figure 9 shows the surface plot diagrams for the depth of hardness. Figure 9 shows that the depth of hardness decreases with increasing laser scanning speed and focal plane position. The reason for this phenomenon is that when the laser scanning speed increases, the workpiece surface is exposed to less heat, and the time of laser interaction decreases, therefore, less energy is absorbed by the surface of the steel. Also with increasing focal plane position, thermal energy entering the surface of the workpiece is reduced (see Figure 1). It is concluded from Figure 9-b and c that with increasing laser power and reducing scanning speed or focal plane position, the depth of the hardened area increases.

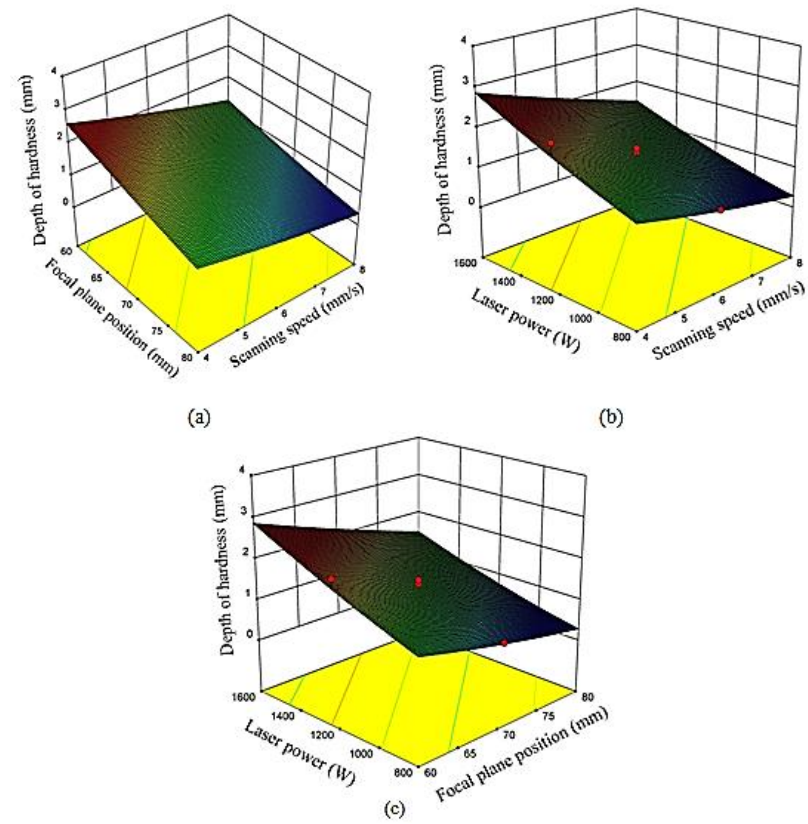

Fig.9 Response surface plots of depth of hardness

The dimension areas of the incidence beam for each focal plane position used in this study are presented in Table 4. When the energy density increases, the austenitic temperature of the steel rises, so the hardness and depth of hardness increases. By using Table 2 and 4, as well as Equation 7, laser beam density is obtained. For samples #13, #14 and #7 as shown in Figure 10, the beam densities are, 37.4 W/mm^2, 21.77 W/mm^2 and 15.50 W/mm^2, respectively.

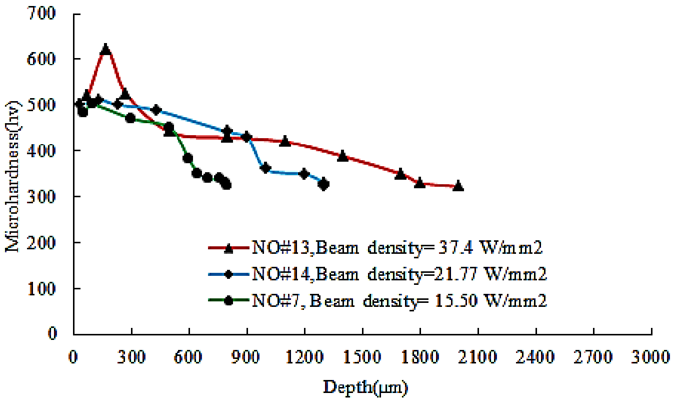

Fig. 10 Microhardness variations in depth based on beam densities

Therefore, with more beam density in sample #13, the depth of hardness of the hardened area will greater. We already know that the energy distribution of the laser beam is rectangular form. This distribution of energy leads to the expansion of the heat affected area, and the hardened area becomes larger, so the depth of hardness of the hardened area is larger than another laser beams that are in the form of gaussian distribution, such as Nd:YAG or fiber lasers. When the shape of the particles are stretched and interconnected in the microstructure, the thermal conductivity and penetration of the laser will increase so the depth of hardness of the hardened area increases. By investigating the microstructure images of the hardened area of AISI 410, it is concluded that the ferrite particles and fine martensite field are stretched, so the thermal energy penetration of the diode laser increases at a depth of the hardened area.

Commented [M19]: Ziad zaroori nist va kaheshehs bedid hatman....

3.3 The Width of hardened area

Table 8 shows a revised ANOVA of width of the hardened area. Laser power, scanning speed, focal plane position are the only significant terms and other terms are in significant. Equations 14 and 15 show the modified linear regression in the form of coded and actual values, respectively:

Commented [M20]: Mesle ghabi

$$(\text{Width of hardness})^{-1.99} = +0.014 - 1.195\text{E-}003S - 1.151\text{E-}003FPP + 1.424\text{E-}003P \quad (14)$$

$$(\text{Width of hardness})^{-1.99} = +0.021422 - 5.97718\text{E-}004S - 1.15129\text{E-}004\ FPP + 3.55987\text{E-}006P \quad (15)$$

Table. 8 Revised analysis of variance of width of hardened area

Source	Sum of squares	Degree of freedom	Mean square	F-value	P-value
Model	1.913E-005	3	6.376E-006	18.52	< 0.0001
S	5.716E-006	1	5.716E-006	16.61	0.0013
P	8.110E-006	1	8.110E-006	23.56	0.0003
FPP	5.302E-006	1	5.302E-006	15.40	0.0017
Residual	4.475E-006	13	3.442E-007		
Lack of fit	4.134E-006	11	3.758E-007	2.21	0.3528
Pure error	3.404E-007	2	1.702E-007		
Total	2.360E-005	16			
	R-Squared= %81.04		Adj R-Squared= %76.67		

3.4 MHD in depth of hardened area

The analysis of variance of the modified model for MHD in depth of hardness is shown in Table 9. The main terms of the scanning speed, laser power and focal plane position, the effect of quadratic terms; scanning speed and laser power, and the interaction of the effects; the scanning speed- laser power and scanning speed- focal plane position are significant in this statistical model. According to the ANOVA, the modified regression Equations 16 and 17 are presented taking into account the effective parameters for the MHD response in the depth of hardness:

Commented [M21]: Mesle ghabl

$$(\text{MHD in depth})^{2.24} = +1.630E{+}009-5.853E{+}008S-6.359{+}008FPP+1.249E{+}009P-8.382E{+}008S\times P-1.145E{+}009S\times FPP+3.996E{+}008S^{2}+8.246E{+}008P^{2} \quad (16)$$

$$(\text{MHD in depth})^{2.24} = -1.64838E{+}010-2.34234E{+}008S+2.79945E{+}008FPP+1.70807E{+}007P-1.04775E{+}006S\times P-2.86281E{+}005S\times FPP+9.99089E{+}007S^{2}+5153.62732P^{2} \quad (17)$$

In Figure 11, the perturbation plot of MHD in depth is shown. Since the laser power parameter in the regression Equation 16 & 17 and its F-Value in ANOVA table are greater than the focal plane position and scanning speed factors, the slope of the laser power curve is more than the other curves. Therefore, laser power has the greatest effect on MHD at hardened depth. Figures 12 show the surface plots of MHD in depth of the hardened area according to the developed regression model.

Commented [M22]: Be tozihate ghabli refer dade she Va ziad keshesh nadim inja

Table 9. Revised analysis of variance of MHD in depth

Source	Sum of Squares	Degree of freedom	Mean square	F-value	P-value
Model	1.126E+019	7	1.608E+018	41.35	< 0.0001
S	1.370E+018	1	1.370E+018	35.23	0.0002
P	6.243E+018	1	6.243E+018	160.54	< 0.0001
FPP	1.618E+018	1	1.618E+018	41.60	0.0001
S × P	3.513E+017	1	3.513E+017	9.03	0.0148
S × FPP	6.557E+017	1	6.557E+017	16.86	0.0027
S^2	2.290E+017	1	2.290E+017	5.89	0.0382
P^2	9.750E+017	1	9.750E+017	25.07	0.0007
Residual	3.500E+017	9	3.889E+016		
Lack of fit	3.491E+017	7	4.987E+016	114.10	0.0087
Pure error	8.742E+014	2	4.371E+014		
Total	1.161E+019	16			
	R-Squared= %96.98		Adj R-Squared=%94.64		

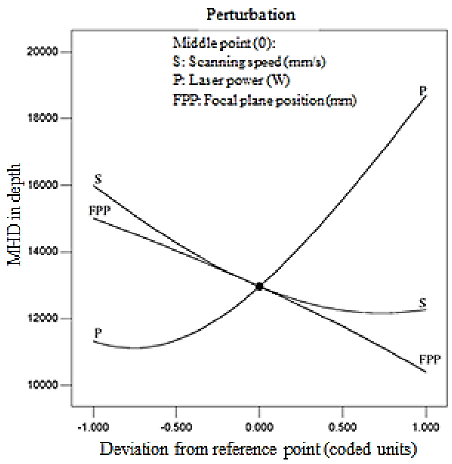

Fig.11 Perturbation plot of the MHD in depth

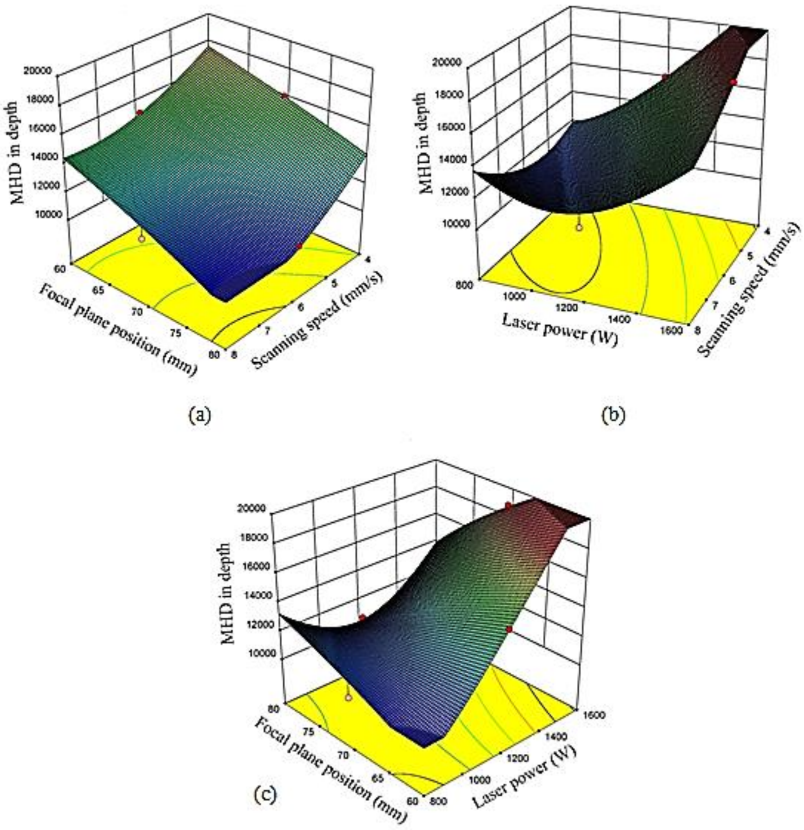

Fig.12 Surface Plot for MHD in depth

It is deduced from Figures 12-a, b, and c that by increasing laser power and reducing the laser scanning speed and focal plane position the MHD in depth increases. As already mentioned, the MHD parameter is directly related to the hardness, so MHD increases with increasing hardness. The reason is that the surface of the workpiece is exposed to more heat and more energy which is absorbed by the surface. It is mentioned in section 3.1 for describing the effect of parameters on maximum hardness. Higher MHD value in hardened sample shows the higher and better uniformity of the hardness distribution in the hardened zone.

Commented [M23]: 2-3 khat she

3.5 MHD in width of hardened area

The variance analysis of the modified model for microhardness deviation from base material (MHD) in width of the hardened area is shown in Table 10. Only the main terms of laser power, focal plane position and scanning speed are known as effective parameters, and other terms are insignificant. Equation 18 and 19 show the final regression equation based on the coded values and actual values for the MHD parameter in the width of the hardened area.

Commented [M24]: Mesle ghabl

$$(\text{MHD in width})^{1.22} = +1.497E+005 - 37723.75S - 48943.95FPP + 80134.64P \quad (18)$$

$$(\text{MHD in width})^{1.22} = +3.65033E+005 - 18861.87736S - 894.39495FPP + 200.33661P \quad (19)$$

Table. 10 Revised analysis of variance of MHD in width

Source	Sum of Squares	Degree of freedom	Mean square	F-value	P-value
Model	4.096E+010	3	1.365E+010	12.95	0.0003
S	5.692E+009	1	5.692E+009	5.40	0.0370
P	2.569E+010	1	2.569E+010	24.35	0.0003
FPP	9.582E+009	1	9.582E+009	9.08	0.0100
Residual	1.371E+010	13	1.244E+009		
Lack of fit	1.368E+010	11	1.244E+009	86.98	0.0114
Pure error	2.860E+007	2	1.430E+007		
Total	5.467E+010	16			
	R-Squared= %84.92		Adj R-Squared = %79.13		

Figure 13 shows the perturbation plot of the MHD in width of the hardened area. It is clear that, with increasing laser power and reducing the focal plane position and scanning speed, the MHD increases in the width of the hardened area. The reason for this is the direct relationship between the MHD parameter and the hardness. Surface plots for MHD in width of the hardened area are shown in Figure 14.

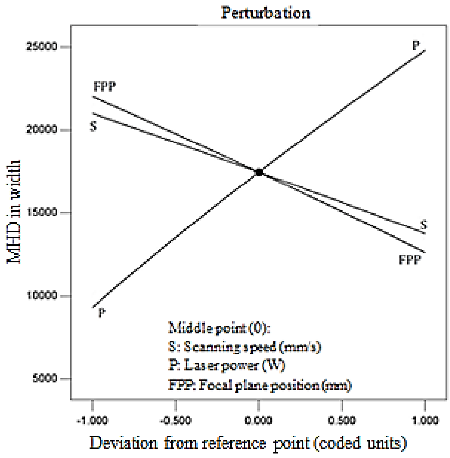

Fig.13 the perturbation plot of the MHD in width

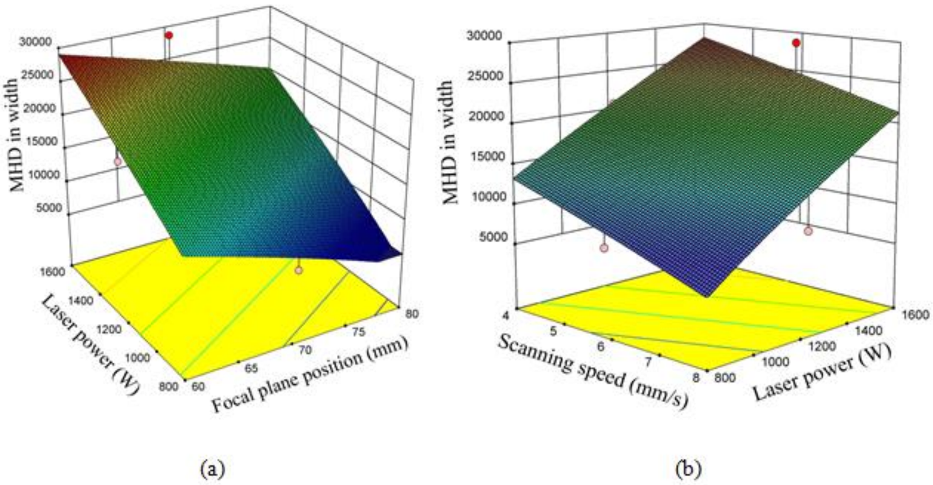

Fig.14 Surface plot for MHD in width

As shown in Figure 14-a, by decreasing the focal plane position and increasing the laser power, the amount of MHD increases. Figure 14-b, shows that with increasing laser power and reducing scanning speed, the MHD value increases in hardened width. The reason for this is that increases in the laser power, and also reduction of the laser scanning speed, the hardened area is exposed to more heat. Therefore, the amount of laser energy entering the surface of the workpiece increases. As a result, the hardness and MHD increase in hardness width. Figure 15 illustrates the variation of MHD in depth and width via microhardness variations.

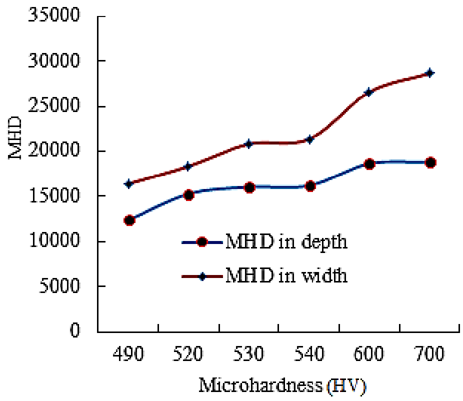

Fig. 15 Comparison of hardness relationship with MHD in the depth and width of the hardened area

Considering that in the laser hardening process of AISI 410, the laser beam profile is rectangular and the density of the beam in the center and the corners is approximately the same, the more uniform hardness in the hardened area will be achieved. The results of the microhardness tests in the hardened area, as well as the MHD analysis, according to Table 2 confirm the uniformity of the diode laser hardened area. As shown in Figure 15, with increasing in hardness, the MHD value increases in the hardened area (in both depth and width), but this increase in the width is greater than in depth. The reason for this is that the shape of the diode laser beam is rectangular. As previously mentioned in MHD in width, the hardness profile is reduced almost uniformly throughout the hardened area and changes of the hardness and MHD in the hardened area are nearly smooth and uniform. With increasing laser beam penetration at a depth of the workpiece, effect of laser energy is gradually reduced at a depth of the workpiece, so, the hardness and MHD in-depth decreases. According to the definition of MHD (see Equation 8), if the hardness points in the hardened area are close together, so the variations in the hardness points selected for the microhardness test are less than the base metal microhardness, and the MHD will be larger. As a result, MHD in width is more than the MHD in depth of the hardened area.

Commented [M25]: Kheili ziade tozihatesh.....

3.6 Ferrite percentage in the microstructure

The modified variance analysis for the percentage of the ferrite phase is shown in Table 11. All of the main terms (laser power, focal plane position and scanning speed) are significant, and other terms are in significant. Equation 20 & 21 show the final regression equation based on the coded values and actual values for the percentage of the ferrite phase**:**

Commented [M26]: Mesle ghablia

$$(\text{Ferrite percent})^{0.24} = +0.081+0.11S+0.011402FPP-0.20P \quad (20)$$

$$(\text{Ferrite percent})^{0.24} = +0.65969+0.040274S+0.011402FPP-5.05385E\text{-}004P \quad (21)$$

Table. 11 Revised analysis of variance of ferrite Percentage

Source	Sum of squares	Degree of freedom	Mean square	F-value	P-value
Model	0.24	3	0.080	6.16	0.0077
S	0.026	1	0.026	1.99	0.1821
P	0.16	1	0.16	12.52	0.0036
FPP	0.052	1	0.052	3.98	0.0674
Residual	0.17	13	0.013		
Lack of fit	0.15	11	0.013	1.08	0.5740
Pure error	0.024	2	0.012		
Total	0.41	16			
R-Squared= %85.72			Adj R-Squared=%77.19		

Figure 16 shows the perturbation plot of ferrite percentage. It is observed that with reducing focal plane position and scanning speed and also with increasing laser power, the percentage of ferrite phase in the structure decreases, due to the increases in the heat input to the workpiece surface and the increase of the steel's austenitic temperature, the ferrite particles are completely dissolved in austenite and a uniform structure including the fine martensite phase and a lower percentage of ferrites are formed.

Ferrite is a soft phase, and it reduces the hardness and strength of the steel. Therefore, identifying and measuring the percentage of ferrite is important. Considering the relationship between the main laser parameters and the percentage of ferrite, it is possible to predict the optimal laser parameters for reducing the ferrite content. Figure 17 shows the relationship between the ferrite percentage and microhardness in hardened laser samples. As can be seen, the ferrite percentage decreases with increasing the hardness.

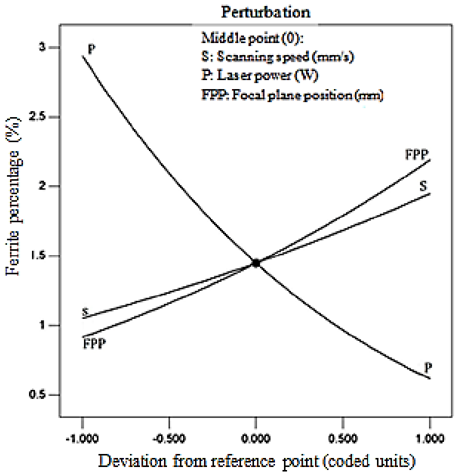

Fig.16 perturbation plot of ferrite percentage

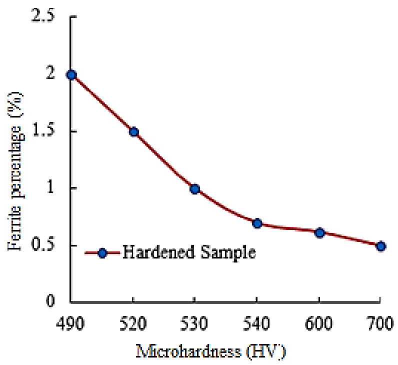

Fig.17 Ferrite percent profile in the hardened samples of diode laser

4. Optimization

In the present study, the results of experimental tests were performed by statistical modeling of the laser surface hardening process using the DOE method. Desirability function has been used to optimize the laser hardening process of AISI 410 to achieve optimum condition. Constraints and criteria for variables and responses are presented in Table 12 to optimize the laser surface hardening process.

Table. 12 Constraints and criteria of input parameters and responses

	Parameter	Goal	Lower	Upper	Importance
Response	Speed	Is in range	4	8	---
	Laser power	Is in range	800	1600	---
	FPP	Is in range	60	80	---
Criteria 1	Surface hardness	Maximize	470	620	5
	Depth of hardness	Maximize	0.5	2.3	5
	Width of hardness	Maximize	8.01	9.2	3
	MHD in depth	Maximize	10204	18658.42	1
	MHD in width	Maximize	7493.2	26621.6	1
	Ferrite percent	Minimize	0.5	3.34	3
Criteria 2	Surface hardness	Maximize	470	620	5
	Depth of hardness	Maximize	0.5	2.3	5
	Width of hardness	Maximize	8.01	9.2	5
	MHD in depth	Maximize	10204	18658.42	1
	MHD in width	Maximize	7493.2	26621.6	1
	Ferrite percent	Minimize	0.5	3.34	1
Criteria 3	Surface hardness	Maximize	470	620	5
	Depth of hardness	Maximize	0.5	2.3	5
	Width of hardness	Maximize	8.01	9.2	-
	MHD in depth	Maximize	10204	18658.42	1
	MHD in width	Maximize	7493.2	26621.6	1
	Ferrite percent	Minimize	0.5	3.34	1

The minimum of ferrite percentage and the maximum value of all other responses are considered for the optimization criteria which are in the three solutions listed in Table 12. The importance values of the output responses are revealed in Table 12.

To validate the optimization results, experimental tests carried out at the optimized settings. Table 13 illustrates the optimal results and the experimental tests. By analyzing the microstructures of the optimized samples and the results obtained from the geometric and microhardness properties, it is concluded that Criteria # 3, has the best response for diode laser surface hardening process AISI 410 in this study. Figure 18 shows the cross-section of optimized laser hardening samples.

Figure 19 shows the microhardness distribution profiles of laser hardened areas in the three optimized samples.

Commented [M27]: In ham mishe 3-4 khatesh konim.... Kholase begidesh

Table. 13 Optimum prediction results and experimental validation

Solution	Optimum input parameters				Composite desirability	Output responses						
		S (mm/s)	FPP (mm)	P (w)			Maximum hardness (HV)	Depth (mm)	Width (mm)	MHD in depth	MHD in width	Ferrite percent (%)
1	Coded value	1.2395	-0.5695	2	0.6921	Actual	580.00	1.80	9	17875	26357	0.52
	Actual value	7.3	66.25	1600		Predicted	603.33	1.94	8.24	19000	27560	0.58
						Error %	-3.86	-7.21	+9.22	-5.92	-4.36	-10.3
2	Coded value	1.3939	-1.4747	2	0.8163	Actual	600.00	2.00	10	20200	30500	0.41
	Actual value	7.4	62.65	1600		Predicted	619.22	2.16	8.11	21480	31850	0.49
						Error %	-3.10	-7.40	+18.9	-5.95	-4.23	-16.3
3	Coded value	-0.4646	-1.3357	2	1	Actual	670.00	2.40	-	22500	35200	0.45
	Actual value	5.54	63.35	1600		Predicted	687.00	2.64	-	23340	36040	0.48
						Error %	-2.47	-9.09	-	-3.55	-2.33	-6.25

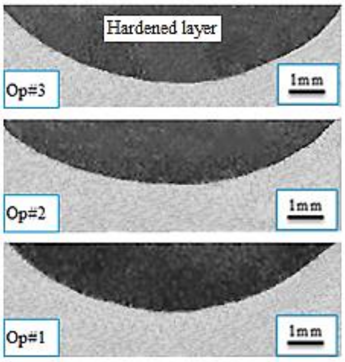

Fig. 18 Cross-section of laser hardening areas in three optimized samples

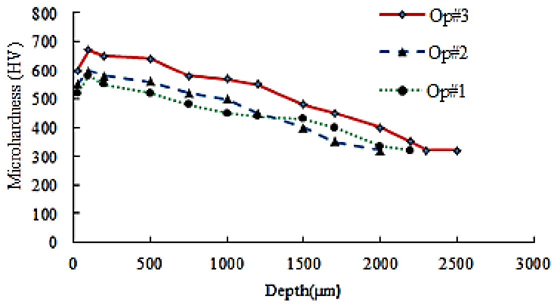

Fig.19 Microhardness profiles of laser hardening areas in the three optimized samples.

Figure 20 shows overlay contour plots in which the contour plots from each output response laid on each other. Every contour Plot is an undesirable gray area and final optimum settings with green area. Overly plot offers a suitable processing window to achieve the desired conditions. In the analyses performed, a parameter that has composite desirability of 1 is the most suitable option. Therefore, the laser power of 1600 w, the scanning speed of 5.54 mm/s and the focal plane position of 63.35 mm is considered as the best setting (sample OPT #3).

Commented [M28]: Chand khat kamtar mitoone beshe be nazaram….

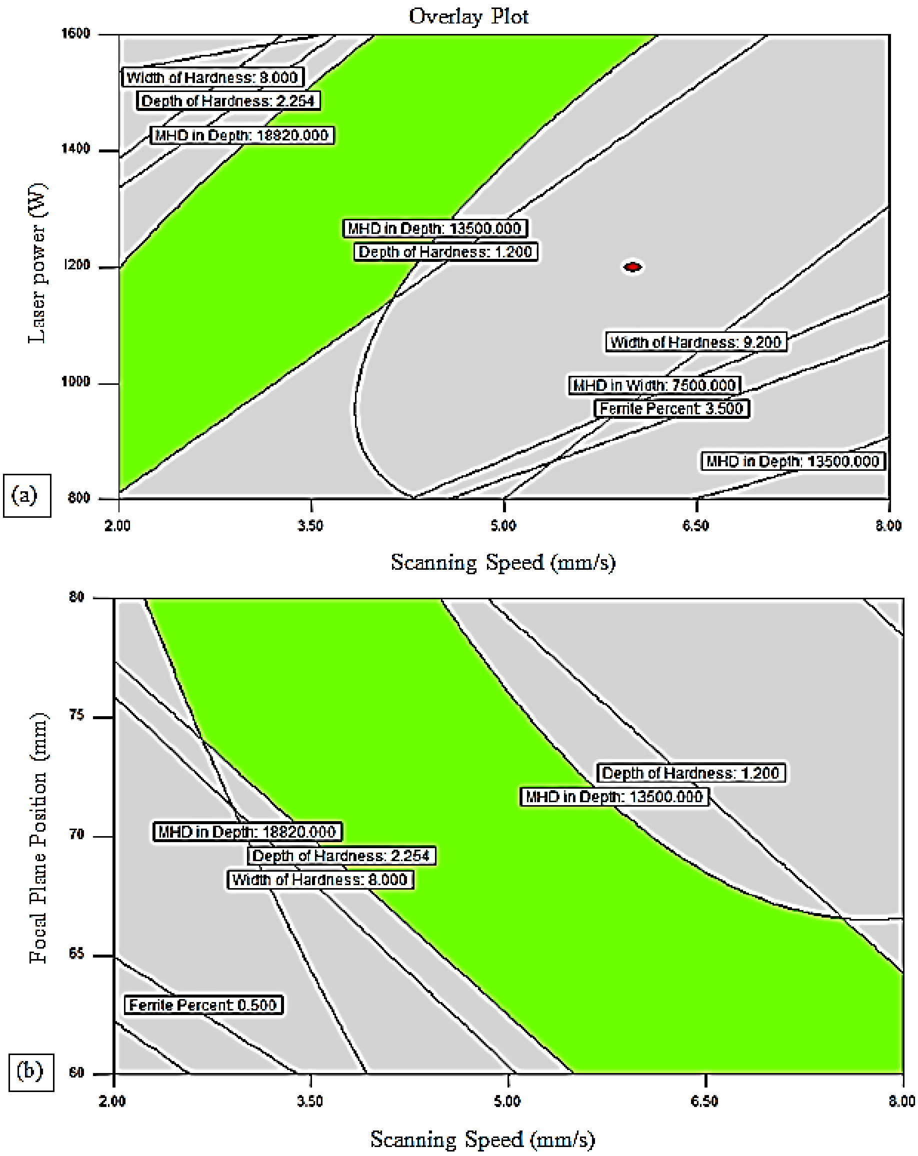

Fig. 20 Overlay contour plot, a) Laser power–Scanning speed, b) Focal plane position- Scanning speed

7. Conclusions

Commented [M29]: Az concolusion ha yeki 2 ta ke kheili badihi ye va khas nist ro hazf konid ke kam she

In the present paper, parameters of diode laser hardening were investigated on the AISI 410 martensitic stainless steel using the DOE method. The following results are obtained from the present study:

1. Results show that with increasing laser power, reducing scanning speed and the focal plane position due to increased laser energy and the amount of heat entering the workpiece surface increases, so value of the hardness and depth of the hardened area increases and also the percentage of ferrite phase in the martensitic field decreases.
2. Results of the measuring grain size show that the grain size of the ferrite and martensite particles in the hardened area of AISI 410 is smaller than the base material. Thus, hardness increases than the base material.
3. The effect and sensitivity of the laser power parameter on the results is more than the focal plane position and scanning speed parameters.
4. By optimizing the process parameters via desire ability approach, the laser optimized parameters with a laser power of 1600 w, scanning speed of 5.54 mm/s and a focal plane position of 63.35mm were proposed.
5. In the best optimum condition, the maximum hardness of 670 Vickers and 2.4 mm hardness depth was achieved.

8. References

1. Budinski, K.G., 1988. Surface Engineering for Wear Resistance, Prentice Hall, New York.
2. Khorram A., Jafari A., Moradi M., 2018. Effect of Linear Heat Input on the Morphology and Mechanical Properties of Ti-6Al-4V Welded Using a CO_2 Laser, Lasers in Engineering, Lasers in Engineering 40 (1-3), 49-64.
3. Sundqvist, J. Kaplan, A. F. H., Granström, J., and Sundin, K.G., 2015. Identifying residual stresses in laser welds by fatigue crack growth acceleration measurement, Journal of Laser Applications, 27, 042002.
4. Moradi M., Ghoreishi M., Rahmani A., 2016. Numerical and Experimental Study of Geometrical Dimensions on Laser-TIG Hybrid Welding of Stainless Steel 1.4418, vol. 5, (2), pp. 21-31.
5. Faraji, A. H., Moradi, M., Goodarzi, M., Colucci, P., 2017. Carmine Maletta. An investigation on capability of hybrid Nd:YAG laser-TIG welding technology for AA2198 Al-Li alloy. Optics and Lasers in Engineering, 96, 1-6.
6. Moradi, M., Ghoreishi, M., & Khorram, A., 2018. Process and Outcome Comparison between Laser, Tungsten Inert Gas (TIG) and Laser-TIG Hybrid Welding. Journal of lasers in Engineering, Vol. 39 (3-6), pp. 379-391.

7. Moradi, M., Golchin E., 2017. Investigation on the effects of process parameters on laser percussion drilling using finite element methodology statistical modelling and optimization, Latin American Journal of Solids and Structures, Vol. 14, No. 03, pp. 464-484.
8. Moradi, M., Abdollahi, H., 2017. Laser Percussion Micro-Drilling on Thin Stainless Steel Sheet AMS 5510; Statistical Modelling and Optimization. Journal of lasers in Engineering, Vol. 39, pp.385- 495.
9. Moradi, M., Mehrabi, O., Azdast, T., Benyounis, K. Y., 2017. Enhancement of low power CO_2 laser cutting process for injection molded polycarbonate. Optics & Laser Technology. Vol. 96, pp. 208–218.
10. Moradi, M., Karami Moghadam, M., Kazazi M., 2019 (February). Improved Laser Surface Hardening of AISI 4130 Low Alloy Steel with Electrophoretically Deposited Carbon Coating, Optik. Vol. 178, pp. 614-622.
11. Abboud, J. H., Benyounis, Julifkar, H., Hashmi, M.S.J., 2017. Material Response With High Power Laser in Surface Treatment of Ferrous Alloys,Materials Science and Materials Engineering. pp. 1-12.
12. Moradi, M., Arabi, H., 2018. Increasing the Surface Hardness of 410 Martensitic stainless Steel Using High Power Diode Laser, Journal of Science and surface engineering, (35) pp: 59-70.
13. Moradi, M., Arabi, H., Jamshidi Nasab, S., Benyounis, K.Y., 2019 (April). A comparative study of laser surface hardening of AISI 410 and 420 martensitic stainless steels by using diode laser. Optics and Laser Technology. Vol.111, pp. 347-357.
14. Oladoye, A.M., Carton, J.G., Benyounis, K.Y., Stokes, J., Olabi, A.G., 2016. Optimization of pack chromised stainless steel for proton exchange membrane fuel cells bipolar plates using response surface methodology Surface and Coatings Technology. 304: 384-392.
15. Abdollahi H., Mahdavinejad R.A., Ghambari M., Moradi M., 2014. Investigation of green properties of iron/jet-milled grey cast iron compacts by response surface method, Proceedings of the Institution of Mechanical Engineers, Part B: Journal of Engineering Manufacture, vol. 228, (4), pp. 493-503.
16. Haddadi, E., Moradi, M., Karimzad Ghavidel, A., Karimzad Ghavidel, A., Meiabadi, S. 2019. Experimental and Parametric Evaluation of Cut Quality Characteristics in CO2 Laser Cutting of Polystyrene, Optik 184, 103-114.
17. Moradi, M., Ghoreishi, M., 2011. Influences of Laser Welding Parameters on the Geometric Profile of Ni-Base Superalloy Rene 80 Weld-Bead. International Journal of advanced manufacturing Technology. Vol. 55, No. 1-4, pp. 205-215.
18. Lo, K.H., Cheng, F.T., & Man, H.C., 2003 (August). Laser transformation hardening of AISI 440C martensitic stainless steel for higher cavitation erosion resistance", Surface and Coatings Technology. Vol. 173, Issue 1, pp. 96–104.

19. Bressan, J.D., Daros, D.P., Sokolowski, A., Mesquita R.A., & Barbosa, C.A., 2008. Influence of hardness on the wear resistance of 17-4ph stainless steel evaluated by the pin-on-disc testing, journal of materials processing technology. Vol. 205, 353–359.
20. Mahmoudi, B., Saboor rooh Aghdam, A.R., & Torkamani, M.J., 2008. Investigating the Effect of laser Parameters on Surface Hardening of Martensitic Stainless Steel 420 by Nd: YAG Laser. 15th Iranian Conference on Optics and Photonics. 8th Iranian Conference on Photonics. Esfahan University.
21. Mahmoudi, B., Saboor rooh Aghdam A.R., & Torkamany, M. J., 2010. Controlled laser transformation hardening of martensitic stainless steel by pulsed Nd:YAG laser, Journal of electronic science and technology.Vol. 8, No. 1, pp. 87-90.
22. badkar, D. s., Panday, K. S., & Buvanashekaran, G., 2010. Effects of laser phase transformation hardening parameters on heat input and hardened-bead profile quality of unalloyed titanium, Transactions of nonferrous Metals Society of China. Vol. 20, pp.1078-1091.
23. Li, R., Jin, Y., Li., Z., & Qi, K., 2014. A Comparative Study of High-Power Diode Laser and CO_2 Laser Surface Hardening of AISI 1045 Steel. Journal of Materials Engineering and Performance.Vol.23 (9), pp. 3085-3091.
24. Cordovilla, F., Garc´ıa-Beltra´n, A., Sancho, P., Dom´ınguez, J., Ruiz de Lara, L., & Oca˜na, J. L., 2016. Numerical experimental analysis of the laser surface hardening with overlapped tracks to design the configuration of the process for Cr-Mo steels. Materials & Design. Vol. 102, pp. 225-237.
25. Li, L., 2000.The advances and characteristics of high-power diode laser materials processing. Optics and Lasers in Engineering. Vol. 34, pp. 231-253.
26. Thelning, K. E., 1984. Steel and Its Heat Treatment, 2nd Edition, Bofors Handbook.
27. Moradi, M., Meiabadi, S., Kaplan, A., 2019. 3D Printed Parts with Honeycomb Internal Pattern by Fused Deposition Modelling; Experimental Characterization and Production Optimization, Metals and Materials International. (Article in press).
28. Kostov, V., Gibmeier, J., & Wanner, A., 2017. Spatially resolved temporal stress evolution during laser surface spot hardening of steel, Journal of Materials Processing Technology. Vol. 239, pp. 326–335.
29. Moradi, M., Mohazabpak, A., 2018. Statistical Modelling And Optimization of Laser Percussion Microdrilling of Inconel 718 Sheet Using Response Surface Methodology (RSM). Journal of lasers in Engineering. Vol. 39 (3-6), pp. 313-331.
30. Moradi, M., Ghoreishi, M., Torkamany, M.J., 2014. Modeling and optimization of Nd:YAG laser-Tig Hybrid welding of stainless steel, Journal of lasers in Engineering. Vol. 27, pp. 211–230.
31. Jenabali Jahromi S.A., Khajeh A., Mahmoudi B., 2012. Effect of different pre-heat treatment processes on the hardness of AISI 410 martensitic stainless steels surface-treated using pulsed neodymium-doped yttrium aluminum garnet laser. Materials and Design, 34, pp. 857–862, 2012.

32. Moradi, M., KaramiMoghadam, M., 2019. High power diode laser surface hardening of AISI 4130; Statistical modelling and optimization, Optics & Laser Technology. Vol. 111, pp.554-570.
33. Elijah Kannatey Asibu, J.r., 2009. Principles of Laser Material Processing, New Jersey: Published by John.
34. Jelokhani-Niaraki, M. R., Mostafa Arab, N. B., Naffakh-Moosavy, H., & Ghoreishi, M., 2016 (June). The systematic parameter optimization in the Nd:YAG laser beam welding of Inconel 625, The International Journal of Advanced Manufacturing Technology. Vol. 84, NO 9–12, pp. 2537–2546.
35. Moradi, M., Fallah, M.M., Jamshidi Nasab, S., 2018. Experimental study of surface hardening of AISI 420 martensitic stainless steel using high power diode laser. Transaction of the Indian institute of metal: Springer Nature. Vol. 71 (8), pp. 1-18.
36. Smallman, R.E., 1990. Modern physical Metallurgy, Furth Edition, Great Britain, The University of Birmingham.